

Quantum-wave evolution in a step potential barrier

Jorge Villavicencio,^{1, 2,*} Roberto Romo,^{2, †} and Sukey Sosa y Silva^{2, ‡}

¹*Instituto de Física, Universidad Nacional Autónoma de México
Apartado Postal 20 364, 01000 México, Distrito Federal, México*

²*Facultad de Ciencias, Universidad Autónoma de Baja California
Apartado Postal 1880, 22800 Ensenada, Baja California, México*

(Dated: October 27, 2018)

By using an exact solution to the time-dependent Schrödinger equation with a point source initial condition, we investigate both the time and spatial dependence of quantum waves in a step potential barrier. We find that for a source with energy below the barrier height, and for distances larger than the penetration length, the probability density exhibits a *forerunner* associated with a non-tunneling process, which propagates in space at exactly the semiclassical group velocity. We show that the time of arrival of the maximum of the *forerunner* at a given fixed position inside the potential is exactly the traversal time, τ . We also show that the spatial evolution of this transient pulse exhibits an invariant behavior under a rescaling process. This analytic property is used to characterize the evolution of the *forerunner*, and to analyze the role played by the time of arrival, $3^{-1/2}\tau$, found recently by Muga and Büttiker [Phys. Rev. A **62**, 023808 (2000)].

PACS numbers: 03.65.-w

I. INTRODUCTION

Since the original proposal by Stevens[1] of tunneling monochromatic fronts, the problem has become controversial and still open to investigations. The existence of such propagating fronts has been supported in asymptotic analysis based on exact analytical solutions [2] to the time-dependent Schrödinger equation, with point source initial conditions. However, analytical and numerical studies based on different boundary conditions and potentials [3], have shown evidence that it is not possible to identify such fronts, in the way suggested in Ref. [2]. Despite these clarifying works, the need of a direct and comprehensive study of the original point source problem has been recently emphasized [4, 5].

A recent study of Muga and Büttiker [5] of quantum waves in a potential step, has shown the existence of a traveling transient *forerunner* for frequencies of the source below the barrier height, which in opaque barrier conditions ($xq_0 \gg 1$) is dominated by over-the-barrier frequencies, implying that this transient structure is associated to a non-tunneling process. They also found that the time of arrival at a fixed position x_f is unexpectedly given by $3^{-1/2}\tau$, where τ is the *traversal time*, defined as $\tau = (x_f/v_{q_0})$, with $v_{q_0} = (\hbar q_0/m)$, and $q_0 = [2m(V_0 - E_0)]^{1/2}/\hbar$; the parameters V_0 and E_0 correspond respectively to the step potential height and the initial energy of the source. We believe that in order to gain more insight about the evolution of quantum waves, the above investigation should be extended to study the role played by τ in the spatial-dependence of the solution.

In this paper we investigate both the time and position dependence of quantum waves in a step potential barrier by means of an exact solution to the time-dependent Schrödinger equation. Our analysis shows that the *forerunner* travels in space at exactly the semiclassical group velocity v_{q_0} , implying that the traversal time τ is exactly the time of arrival of the maximum of the *forerunner* at a fixed point deep inside the potential step; clearly this result is different from the time scale of Ref. [5] by a factor of $3^{-1/2}$. Using a scaling property of the *forerunner* derived from the analytic solution, the exact interpretation of the time scales τ and $3^{-1/2}\tau$ as times of arrival is clarified. It is a surprising fact that τ , a time scale traditionally regarded as one of the possible tunneling times, is here associated to a non-tunneling process.

This work is organized as follows. Section II deals with numerical examples, showing both spatial and time evolution of the probability density for initial waves with energies $E_0 > V_0$, and $E_0 < V_0$. Finally, the conclusions are presented in Section III.

II. QUANTUM WAVE EVOLUTION

In this section we shall explore the main features of quantum wave evolution. Here we use the exact analytical solutions [2, 5] (see also Appendix A) to the time-dependent Schrödinger equation for a step potential barrier $V(x) = \Theta(x)V_0$, for a wave formed by a point source with a sharp onset,

$$\psi_0(x = 0, t) = \begin{cases} e^{-i\omega_0 t}, & t > 0, \\ 0, & t < 0. \end{cases} \quad (1)$$

We have defined $\omega_0 = (E_0/\hbar)$, where E_0 corresponds to the initial energy of the source. It is worthwhile to point out that the source boundary condition given by Eq. (1) is not a standard one in quantum mechanics.

*Electronic address: villavics@uabc.mx

†Electronic address: romo@uabc.mx

‡Electronic address: sukeys@hotmail.com

For a physical interpretation of these type of boundary conditions see Ref. [7].

The analytical solutions for the point source problem are given by,

$$\psi_>(x, t) = e^{-iVt} [M(x, k_0, t) + M(x, -k_0, t)], \quad \omega_0 > V, \quad (2)$$

and,

$$\psi_<(x, t) = e^{-iVt} [M(x, iq_0, t) + M(x, -iq_0, t)], \quad \omega_0 < V, \quad (3)$$

where $k_0 = [2m(\omega_0 - V)/\hbar]^1/2$, $q_0 = ik_0$, and $V = (V_0/\hbar)$. In the above equations the M -functions are defined as,

$$M(x, q, t) \equiv M(y_q) = \frac{1}{2} e^{imx^2/2\hbar t} w(iy_q), \quad (4)$$

where w is the complex error function [10, 11] $w(z) = \exp(-z^2) \operatorname{erfc}(-iz)$. The argument y_q in Eq. (4) is given by,

$$y_q = e^{-i\pi/4} \left(\frac{m}{2\hbar t} \right)^{1/2} \left[x - \frac{\hbar q}{m} t \right], \quad (5)$$

where $q = \pm k_0, \pm iq_0$.

From the analysis given in Subsection A.1, one can obtain the long time behavior of Eqs. (2) and (3). For the long time regime $t \rightarrow \infty$ the asymptotic solutions are,

$$\psi_<^a(x, t) = e^{-i\omega_0 t} e^{-q_0 x}, \quad \omega_0 < V, \quad (6)$$

and

$$\psi_>^a(x, t) = e^{-i\omega_0 t} e^{-ik_0 x}, \quad \omega_0 > V. \quad (7)$$

In what follows we shall explore the main features of waves along the potential region, $x > 0$, generated by a source with the initial frequencies $\omega_0 > V$ and $\omega_0 < V$. Our emphasis will be in the second case, where we shall reveal novel aspects in the spatial evolution of quantum waves.

A. Source with an initial frequency $\omega_0 > V$

Although the main purpose of the present work is to explore the dynamics of the solution for a source with an initial frequency $\omega_0 < V$, for completeness we begin our discussion by illustrating some cases for $\omega_0 > V$. In this subsection we investigate the evolution of the solution given by Eq. (2). We choose the following parameters for the system: height of the potential step, $V_0 = 1.0$ eV, and the energy of the initial wave, $E_0 = 2.0$ eV. The calculated values of $|\psi_>|^2$ are shown in Fig. 1 (a) as a function of the position x , for two fixed times $t_1 = 15.0$ fs, and $t_2 = 30.0$ fs. It is clearly appreciated in Fig. 1 (a), that a main wavefront with damped oscillations is propagating from left to right. One can easily verify

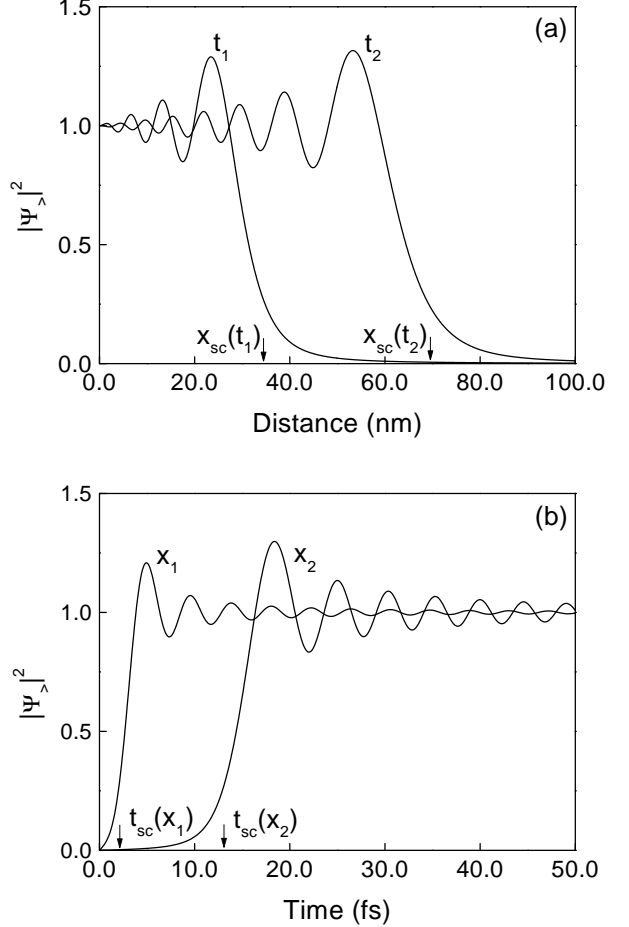


FIG. 1: (a) Spatial evolution of $|\psi_>|^2$, for two different values of time: $t_1 = 15.0$ fs, and $t_2 = 30.0$ fs. The positions $x_{sc}(t_i) = v_{k_0} t_i$ of the semiclassical fronts are indicated by an arrow in each curve. (b) Time evolution of $|\psi_>|^2$ at different fixed positions $x_1 = 5.0$ nm and $x_2 = 30.0$ nm, in order to show the wavefront propagation. The positions $t_{sc}(x_i) = (x_i/v_{k_0})$ of the semiclassical fronts are also indicated by an arrow. Notice how as time increases the solution tends to the correct asymptotic value given by $|\psi_>^a|^2 = 1$.

by numerical inspection that the main wavefront travels approximately with the semiclassical group velocity $v_{k_0} \simeq \hbar k_0/m$. The arrows in Fig. 1 (a) indicate the semiclassical positions $x_{sc}(t_i) = v_{k_0} t_i$, ($i = 1, 2$).

The plots of $|\psi_>|^2$ vs t , for a two different fixed positions $x_1 = 5.0$ nm and $x_2 = 30.0$ exhibited in Fig. 1 (b), complement our discussion for this case. Here we also illustrate the propagation of the main wavefront for the specific positions x_i indicated in the figure. Notice how the probability density rises from zero and grows monotonically towards a maximum value, from which it starts to oscillate until it reaches the stationary value. This sudden rise occurs approximately at times $t_{sc}(x_i) = (x_i/v_{k_0})$, which correspond to the arrival of the main wavefront at the fixed position x_i . It is interesting

to mention that these propagation features are similar to the *diffraction in time* patterns observed in free particle propagation within the Moshinsky shutter model[8], which is in fact a different type of initial condition.

Although we see that in the case $\omega_0 > V$ it is permissible to speak of a propagation of a main wave front, the issue has become controversial in case of initial waves with $\omega_0 < V$ [1, 2, 4, 5, 12]. The results for this more complicated case is discussed in the next subsection.

B. Source with an initial frequency $\omega_0 < V$

In what follows we shall explore the main features of the time and spatial behavior of the probability density for a source with an initial frequency $\omega_0 < V$. We consider here the same potential parameters as in the previous subsection, but the energy is now chosen below the height of the barrier, $E_0 = 0.5$ eV. In Fig. 2 (a) we show the time evolution of $|\psi_<|^2$ at the positions $x_1 = 1.2$ nm and $x_2 = 1.5$ nm. Notice that the curves exhibit a behavior similar to the diffraction in time pattern observed in the previous subsection. As we shall discuss below, this behavior is not related to the propagation of a main wave front, and requires a different interpretation. In fact, the time-diffraction-like pattern disappears after a certain depth inside the potential, where the probability density exhibits now a pulse-like structure, as can be appreciated in Fig. 2 (b).

In order to understand the transition between the quite different dynamical behavior of $|\psi_<|^2$ observed in Fig. 2 (a) and (b), a series of snapshots of $|\psi_<|^2$ vs x are shown in Fig. 3 (solid lines) for increasing values of time. We can appreciate in Fig. 3 (a) that at short times the probability density behaves like the stationary solution $|\psi_<^a|^2$ (dashed line) along the internal region. However, the probability density, $|\psi_<|^2$, dramatically changes as time elapses. This is depicted in Fig. 3 (b), where we see the appearance of a bump for values of the position x larger than X_0 . This special point X_0 corresponds to the onset of a pulse-like structure that we call *transient pulse* (forerunner). In Figs. 3 (c) and (d), the transient pulse is now fully formed, and propagates along the region $x > X_0$. However, notice that as time increases, the birth of the pulse occurs at values of the position X_R , greater than value of the lower-bound, X_0 . The positions X_0 (full square) and X_R (full dot) are indicated in Fig. 3. We have systematically studied this transition for different potential steps, as well as for different energies of the initial waves, and our results indicate that the onset of the *transient pulse* always occurs at a specific depth, X_0 , inside the potential, which is twice the value of the characteristic *penetration length* $x_p = q_0^{-1}$ of the stationary solution: $X_0 \approx 2x_p$. The existence of this two regimes for the point source model has also been reported in Ref. [6]. A similar separation into two regimes, but in different models has been observed by one of the authors in Refs. [12, 13].

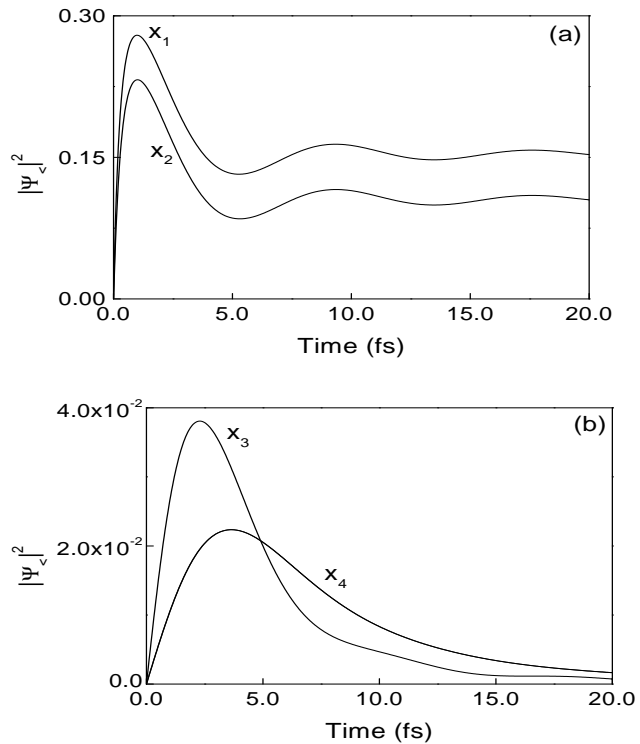


FIG. 2: Time evolution of $|\psi_<|^2$, at different values of the position along the internal region. Notice that (a) at the fixed positions $x_1 = 1.2$ nm, and $x_2 = 1.5$ nm, the probability density exhibits an oscillating behavior similar to the diffraction in time phenomenon. At the positions (b) $x_3 = 6.0$ nm, and $x_4 = 10.0$ nm, located deep inside the internal region, the oscillating pattern no longer exists, and it is replaced by a pulse-like structure.

We shall later see that the approximate value of X_R can be determined approximately by using a simple analytical formula. In what follows we shall explore in more detail the regimes $0 < x < X_0$, and $x > X_0$. We shall refer to the latter as the *transient pulse regime*.

1. $0 < x < X_0$ regime

This regime corresponds to short distances inside the potential, namely, to positions x such that $0 < x < X_0$. Here we shall explain the oscillatory patterns of the $|\psi_<|^2$ vs t plots, observed within this finite interval and exhibited in Fig. 2 (a). We shall see that, rather than originated by the passage of a traveling wavefront (as it occurs in the case $\omega_0 > V$), this effect is due to fluctuations of the probability density. This dynamical behavior is illustrated in Fig. 4, where we present a series of snapshots of $|\psi_<|^2$ vs x , for increasing values of time indicated in the figure. Here we have included for comparison the calculation of the stationary probability density $|\psi_<^a|^2$ (dashed line). Notice that the evolution of the time dependent probability density occurs in such a

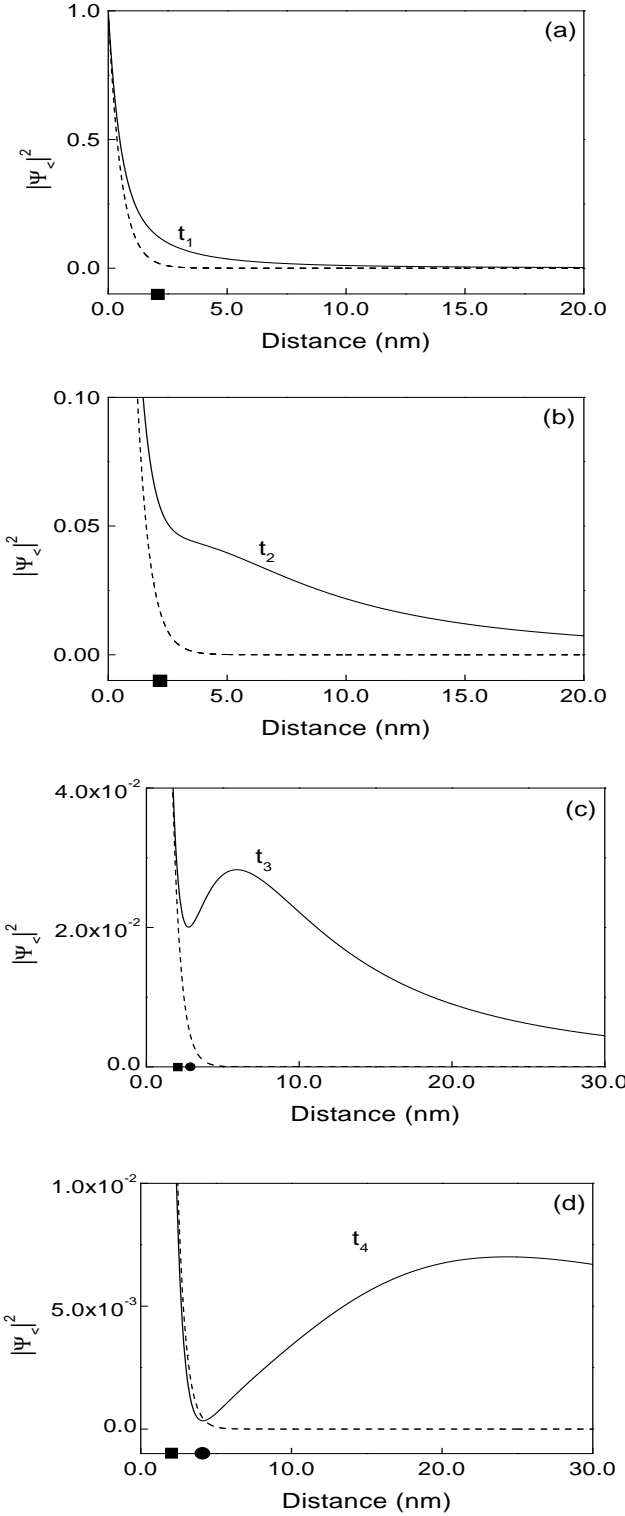


FIG. 3: Birth of the probability density $|\psi_{<}|^2$ (solid line) as function of the distance x , for increasing values of time: $t_1 = 1.0$ fs, $t_2 = 3.0$ fs, $t_3 = 4.0$ fs, and $t_4 = 15.0$ fs. In part (a), we see a monotonically decreasing curve. However, a bump begins to appear in (b), which corresponds to the birth of a *transient pulse*. In (c) and (d), the maximum of this pulse propagates along $x > X_0$. In all cases, the stationary solution $|\psi_{<}^a|^2$ (dashed line) is included for comparison. A full square and a dot indicate the position of $X_0 = 2.134$ and X_R , respectively.

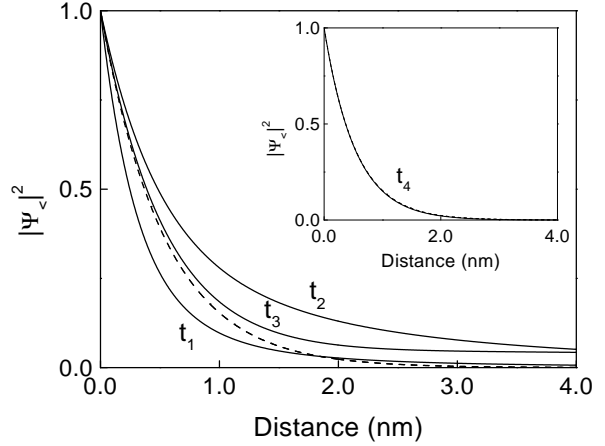


FIG. 4: Plot of $|\psi_{<}|^2$ as a function of the position at different values of time: $t_0 = 1.0$ fs (solid line) $t_1 = 2.0$ fs (dotted line), and $t_2 = 3.0$ fs (dashed-dotted line). The stationary solution $|\psi_{<}^a|^2$ (dashed line) is also included for comparison. The inset shows $|\psi_{<}|^2$ (solid line) at a later time $t_3 = 15.0$ fs, which becomes indistinguishable from the stationary solution (dashed line).

way that $|\psi_{<}|^2$ is found sometimes above or below the asymptotic value. This illustrates that, in this regime, the probability density fluctuates around the stationary solution before reaching its asymptotic limit. At long enough times, we must have $|\psi_{<}|^2 \rightarrow |\psi_{<}^a|^2$, which is illustrated in the inset of Fig. 4, where for $t = 15.0$ fs both curves become indistinguishable.

The above results are relevant since they clearly show that we can not associate in this regime a semiclassical group velocity to the main wave-front towards its steady state. In other words it is not possible to define a semiclassical main front attenuated exponentially by $e^{-q_0 x}$, traveling along the internal region with a group velocity $v_{q_0} = (\hbar q_0 / m)$, as suggested by Moretti [2]. However, a special kind of propagation actually exists for $x > X_0$ (opaque barrier conditions), which consists of the traveling forerunner mentioned in the Section I. It should be emphasized however that this transient structure (in view of its frequency content) is not associated to a tunneling process[5]. We shall show in the next subsection that the maximum of this *forerunner* travels at exactly the group velocity, v_{q_0} .

2. Transient pulse regime ($x > X_0$)

This regime corresponds to the case $x > X_0$, where the dynamics of the probability density $|\psi_{<}|^2$ is governed by a *transient pulse*. This transient structure originates from X_0 onwards, and evolves thereafter along $x > X_0$, as depicted in figures 3 (c) and 3 (d). In Fig. 5 (a), we plot $|\psi_{<}|^2$ vs x for the increasing values of time: $t_0 = 30.0$ fs, $t_1 = 100.0$ fs, $t_2 = 150.0$ fs, and $t_3 = 300.0$ fs. Here, no

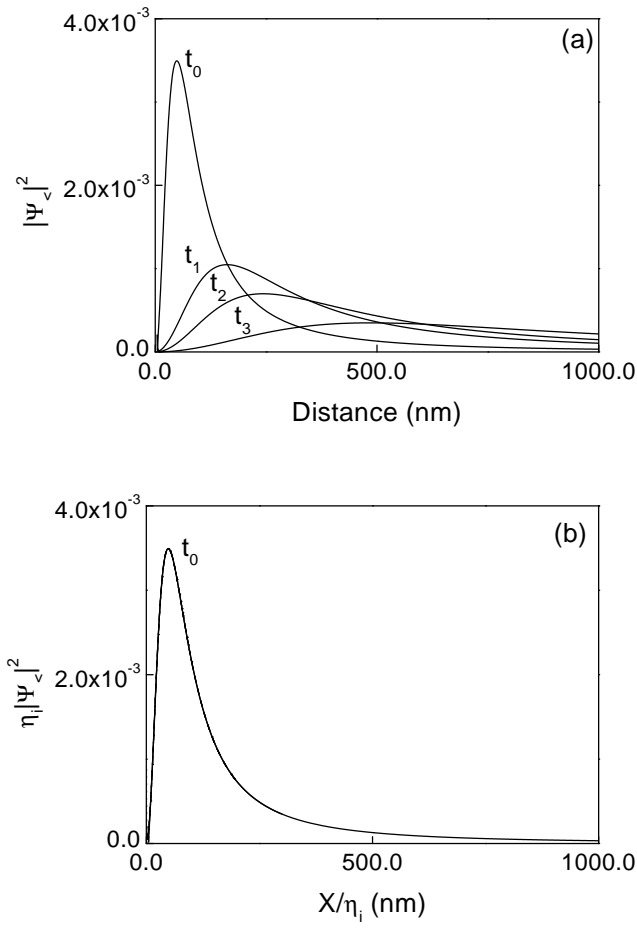


FIG. 5: (a) Spatial evolution of the *transient pulse* calculated from $|\psi_<|^2$ for increasing values of time: $t_0 = 30.0$ fs, $t_1 = 100.0$ fs, $t_2 = 150.0$ fs, and $t_3 = 300.0$ fs. Notice the different values of the pulse peak and width for each particular time. (b) Plot of the rescaled probability density $\eta_i |\psi_<|^2$ ($i = 1, 2, 3$) as function of a variable x/η_i , for the same cases depicted in (a). All curves become indistinguishable and coincide with the $|\psi_<|^2$ vs x plot of the case $t = t_0$. Also included here is a plot of Eq. (13), which, as expected, coincides exactly with all the curves.

traveling main front is observed, as in the $\omega_0 > V$ case. Instead, we see a forerunner that broadens as it travels along the internal region, with diminishing amplitude, similar to the propagation and spreading of a wavepacket.

In addition to the above, the evolution of the probability density in this regime, has an interesting scaling property. If we express the times t_i ($i = 1, 2, 3$) as multiples of t_0 , namely $t_i = \eta_i t_0$ (in our examples: $\eta_1 = 3.333$, $\eta_2 = 5.0$, and $\eta_3 = 10.0$), and use the factors η_i to renormalize both axis, in such a way that we now plot $\eta_i |\psi_<|^2$ vs (x/η_i) , a striking result is obtained: all curves coincide. This invariance under scaling is illustrated in Fig. 5 (b), where all the curves corresponding to $i = 1, 2, 3$, are indistinguishable among them, coinciding with the curve

$|\psi_<|^2$ vs x corresponding to t_0 .

The scaling property illustrated above by means of a numerical example, can also be explained using our analytic formulas. However, instead of using the formal solution given by Eq. (3), we shall first derive a simple expression for the spatial evolution of $|\psi_<|^2$. Notice that the behavior of $|\psi_<|^2$ is essentially governed by two M functions, namely, $M(y_{iq_0})$ and $M(y_{-iq_0})$. By a numerical inspection we find that the series of the M functions discussed in Subsection 1 of Appendix A, apply in this regime. In order to exploit the analytical properties of the Moshinsky functions, first we have to determine the location in the complex-plane of the phases $\phi_{\pm iq_0}$ of the arguments $y_{\pm iq_0}$. We find that the phase ϕ_{-iq_0} , is always within the interval $-\pi/2 < \phi_{-iq_0} < \pi/2$. Thus the series representation given by Eq. (A10a) applies in this case. Similarly, we find that although the phase ϕ_{iq_0} , may change from $\pi/2 < \phi_{iq_0} < 3\pi/2$ to $-\pi/2 < \phi_{iq_0} < \pi/2$ in the vicinity of the maximum of the *transient pulse*, the series representation of the M functions given by Eq. (A11a) gives an excellent approximation. Therefore, we find that in this regime, the behavior of the probability density is essentially governed by the first terms of the series representation of Eqs. (A10a) and (A11a). That is,

$$M(y_{-iq_0}) \simeq \frac{1}{2} e^{imx^2/2\hbar t} \left[\frac{1}{\pi^{1/2} y_{-iq_0}} \right], \quad (8)$$

and

$$M(y_{iq_0}) \simeq \frac{1}{2} e^{imx^2/2\hbar t} \left[2e^{y_{iq_0}^2} + \frac{1}{\pi^{1/2} y_{iq_0}} \right]. \quad (9)$$

After substituting the above expressions in Eq. (3), and performing a few algebraical manipulations, we obtain the following expression for the probability density,

$$\psi_< \simeq \psi_<^a + \psi_{tp}, \quad (10)$$

where $\psi_<^a$ is the stationary solution given by Eq. (6), which decays exponentially along the internal region. Here ψ_{tp} stands for,

$$\psi_{tp} = \frac{1}{2\pi^{1/2}} e^{i(mx^2/2\hbar t - Vt)} \left[\frac{1}{y_{iq_0}} + \frac{1}{y_{-iq_0}} \right], \quad (11)$$

which as we shall see below, accurately describes the *transient pulse*. We have found by numerical inspection that Eq. (10) gives an excellent description of the spatial evolution of $|\psi_<|^2$, provided that $t > (X_0/v_{q_0})$. The result given by Eq. (10) shows us that the probability density can be described by a subtle interplay between $\psi_<^a$ and ψ_{tp} . A measure of such an interplay can be given by the ratio $R = |\psi_<^a/\psi_{tp}|^2$. We have found that the observed transition discussed in Fig. 3, occurring at X_R , corresponds to values of the position such that condition $R = 1$ is satisfied.

If we now focus our attention in describing the dynamics of the pulse, from Eq. (11) we can obtain a simple

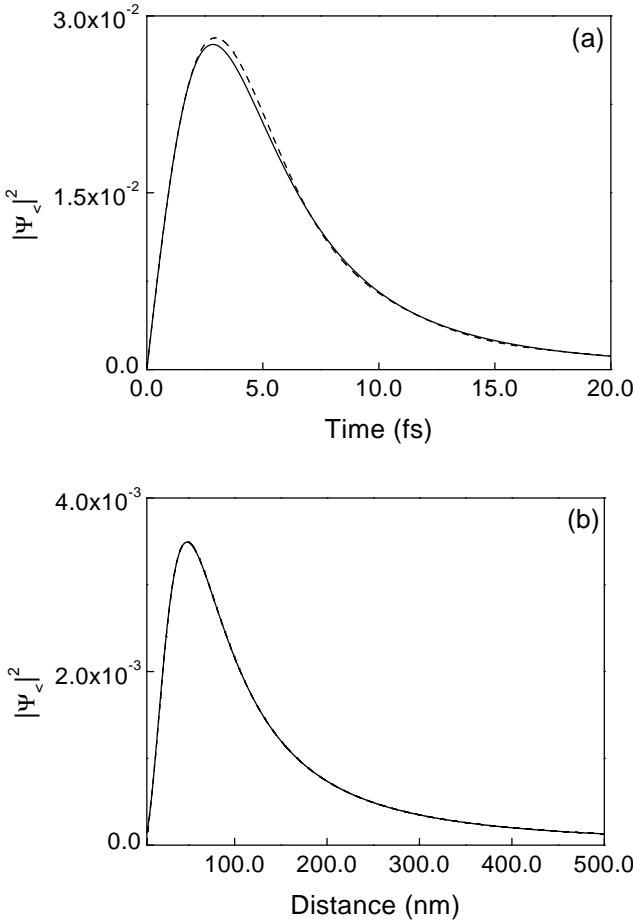


FIG. 6: Comparison of $|\psi_{tp}|^2$ (solid line) and $|\psi_<|^2$ (dashed line), (a) as a function of time, for $x_0 = 8.0$ nm, and (b) as a function of position, for $t_0 = 30.0$ fs; in this case, both curves overlap, and become indistinguishable among them.

analytical expression for this transient structure, namely,

$$|\psi_{tp}(x, t)|^2 = \frac{2}{\pi} \frac{(\hbar x^2 t / m)}{[x^2 + (\hbar q_0 t / m)^2]^2}. \quad (12)$$

The analysis from Eq. (8) to Eq. (12), is equivalent to the one performed in Ref. [5] in terms of a pole and a saddle-point contribution, with a different notation and terminology. It can be appreciated in Fig. 6 (a), that Eq. (12) provides an excellent description for the propagating pulse. Here, we have plotted $|\psi_{tp}|^2$ (solid line) as a function of time at a fixed position $x = 8.0$ nm, and the curve almost coincide with the calculated with the formal solution, Eq. (3) (dashed line). We also compare Eqs. (3) and (12) with a plot of the probability density as a function of position, see Fig. 6(b), and an the description of our approximate formula is excellent, since both calculations are indistinguishable in the graph.

In order to show the scaling property, we make in Eq.

(12) the general substitution of $t' = \eta t$ and $x' = \eta x$. The result of this rescaling is the following equation,

$$|\psi_{tp}(x', t')|^2 = \frac{2}{\eta \pi} \frac{(\hbar x^2 t / m)}{[x^2 + (\hbar q_0 t / m)^2]^2}. \quad (13)$$

A plot of Eq. (13) is also included in Fig. 5 (b), which as expected becomes also indistinguishable from the rest of the curves. From the comparison of Eq. (12) and Eq. (13), the scaling property can be written as,

$$\eta |\psi_{tp}(\eta x, \eta t)|^2 = |\psi_{tp}(x, t)|^2. \quad (14)$$

In what follows we shall apply Eqs. (12) and (14) to analyze the speed of the propagating pulse. In particular, we contrast the propagation of the peak value of the probability density obtained by deriving it with respect to time, to the peak value obtained by deriving with respect to position. As we shall show below, the corresponding speeds differ by a factor of $3^{1/2}$.

The maximum value of $|\psi_{tp}|^2$ at any given point can be obtained straightforwardly by deriving Eq. (12). However, the following results show that the calculation of a maximum of $|\psi_{tp}|^2$ critically depends on whether the spatial or time evolution of the probability density is analyzed. From $(d/dt)|\psi_{tp}|^2 = 0$, we obtain the critical time which maximizes $|\psi_{tp}|^2$ at x_f , the result is,

$$t_m = \frac{\tau}{\sqrt{3}}, \quad (15)$$

where $\tau = (x_f / v_{q_0})$. This result is in exact agreement with the scale found recently by Muga and Büttiker [5] for the time of arrival.

It is clear that the pair (x_f, t_m) gives the maximum value in a $|\psi_{tp}|^2$ vs t plot. However, it is easy to show that the value x_f does not correspond to the position of the peak of the traveling pulse. The latter, which is the maximum of a $|\psi_{tp}|^2$ vs x plot, is in fact located at the left of x_f (see below). From $(d/dx)|\psi_{tp}|^2 = 0$, at a fixed time $t = t_f$, we obtain the maximum of the *transient pulse* as it propagates along the x coordinate, it becomes,

$$x_m = v_{q_0} t_f. \quad (16)$$

Notice that for the particular case $t_f = t_m$, the maximum of the pulse x_m is retarded with respect to x_f i.e. $x_m = 3^{-1/2} x_f$. In other words, the maximum intensity of $|\psi_{tp}|^2$ is attained at x_f , before the arrival of the pulse's peak takes place. Although the above statement seems to be in contradiction, we shall show below that these two types of maximum values have different meanings, and consequently there is no contradiction at all. The values of the probability density at these two positions are illustrated on the $|\psi_{tp}|^2$ vs x plot (solid line) depicted in Fig. 7; they are compared at the same time, $t_m = 30$ fs. The values of $|\psi_{tp}|^2$ at x_m and x_f are indicated on the curve by a full dot and a hollow circle, respectively. Equation (16) shows that the maximum of the pulse (full dot) travels at exactly the semiclassical group velocity v_{q_0} , while

the other (hollow circle), according to Eq. (15), travels faster than the former, at the speed $3^{1/2}v_{q_0}$. In fact, the observed spreading of the pulse is due to the fact that all the points of the $|\psi_{tp}|^2$ vs x curve are traveling with different velocities.

It is clear from Fig. 7 that the height of the hollow circle $h_{hc}(t_m)$ is smaller than the corresponding height of the full dot, $h_{fd}(t_m)$. However, the height of the pulse diminishes at such a rate, that when the full dot reaches x_f at a later time $t' = 3^{1/2}t_m$, its height $h_{fd}(t')$ is smaller than $h_{hc}(t_m)$. This is illustrated in Fig. 7 where we plot $|\psi_{tp}|^2$ as a function of the position x , at a time $t = t'$ (dashed line). The above effect can be easily shown by using the scaling property, Eq. (14). But first, let's us obtain the values of the heights h_{hc} and h_{fd} measured at $t = t_m$, namely,

$$h_{hc}(t_m) = |\psi_{tp}(x_f, t_m)|^2 = \frac{3}{4} \left(\frac{1}{2\pi} \frac{1}{x_m q_0} \right); \quad (17)$$

and

$$h_{fd}(t_m) = |\psi_{tp}(x_m, t_m)|^2 = \left(\frac{1}{2\pi} \frac{1}{x_m q_0} \right). \quad (18)$$

If we now feed $\eta = 3^{1/2}$ in Eq. (14), using the fact that $t' = 3^{1/2}t_m$ and $x_f = 3^{1/2}x_m$, we obtain that $3^{1/2}h_{fd}(t') = h_{fd}(t_m)$. This allows us to write the height ratio as,

$$\frac{h_{hc}(t_m)}{h_{fd}(t')} = \frac{3\sqrt{3}}{4} > 1. \quad (19)$$

Thus, we have in general demonstrated that the maximum value of $|\psi_{tp}|^2$, measured at a fixed position x_f , is always reached there before the arrival of the maximum of the transient forerunner at that particular position. In view of this result, the role of the different time scales is now clear. While the traversal time τ does in fact correspond to the time of arrival of the maximum of the transient forerunner at x_f , the time scale $3^{-1/2}\tau$ corresponds to the attainment of the maximum value of $|\psi_{tp}(x_f, t)|^2$ at x_f , which as demonstrated above, is always associated to values of the probability density located at the front tail of the forerunner.

The above discussion shows that the calculation of the time of arrival may critically depend on whether the spatial or the time evolution of the probability density is analyzed. Although the interpretation of the results is different in each case, we believe that both kind of analysis are important and complementary. It is important to point out that a time-frequency analysis of the *forerunner*, performed in Ref. [5], has revealed that it is composed predominantly by over-the-barrier (non-tunneling) frequencies.

III. CONCLUSIONS

The issue of spatial and time dependence of quantum waves in a step potential barrier has been analyzed

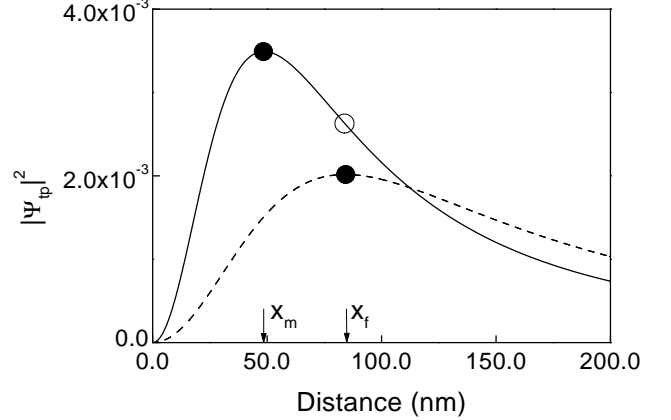


FIG. 7: Spatial evolution of the *transient pulse* calculated from $|\psi_{tp}|^2$ for $t_m = 30.0$ fs (solid line). Its values at the positions $x_m = 48.639$ nm and $x_f = 84.246$ nm are indicated respectively by a full dot and a hollow circle on the solid line. At a later time, $t' = 3^{1/2}t_m$, the maximum of the forerunner reaches the position x_f , as indicated by the full dot on the dashed line. Notice the reduction of its height

by means of an exact solution to the time-dependent Schrödinger equation, for a point source initial condition. The main results of our study are the following: (1) For the case $\omega_0 < V$ in the opaque barrier regime ($xq_0 \gg 1$), we found that the peak of the *forerunner* travels at exactly the group velocity $v_{q_0} = (\hbar q_0/m)$, which implies that the time of arrival of the maximum of the peak at a fixed position in space x_f , is given by the traversal time $\tau = (x_f/v_{q_0})$. This is in contrast to the time scale $3^{-1/2}\tau$ described in Ref. [5]. (2) We derived from the formal solution a closed analytical formula that accurately describes the dynamics of the *forerunner*, and found that it obeys an interesting and useful scaling property. (3) Although $3^{-1/2}\tau$ actually corresponds to the maximum of the *forerunner* when it is analyzed as a function of time (and fixed x), we demonstrated by means of the scaling property that this time scale always correspond to the passage of the front tail (not the maximum) of the forerunner across the fixed position x_f .

As a final remark, it is important to point out that the *forerunner* is mainly composed by over-the-barrier (non-tunneling) frequencies, as recently shown by Muga and Büttiker [5]. Thus, it is a surprising fact that the traversal time τ , usually regarded as one of the possible tunneling times, is here associated to a non-tunneling process.

Acknowledgments

The authors, J. V. and R. R., acknowledge financial support from Conacyt, México, through Contract No. 431100-5-32082E. The authors thank Alberto Hernández

for useful discussions.

APPENDIX A: POINT SOURCE PROBLEM

In this appendix we shall present a different derivation of the solutions to the point source problem [2, 5], by means of the Laplace Transform method. Let us consider an exact analytical solution to the time-dependent Schrödinger equation for a step potential barrier $V(x) = \Theta(x)V_0$,

$$\left[-\frac{\hbar^2}{2m} \frac{\partial^2}{\partial x^2} + V(x) - i\hbar \frac{\partial}{\partial t} \right] \psi(x, t) = 0, \quad (\text{A1})$$

subject to the source boundary condition given by Eq. (1). We must also assume that inside the barrier ($x \geq 0$) the initial state ψ_0 satisfies the boundary condition $\psi_0(x; t = 0) = 0$, for $x \geq 0$.

To obtain the solution for $x > 0$ at $t > 0$, we begin by Laplace transforming equation (A1) using the standard definition

$$\bar{\psi}(x; s) = \int_0^\infty \psi(x, t) e^{-st} dt, \quad (\text{A2})$$

with the initial condition given by Eq. (1). Let us first consider the case propagating waves ($\omega_0 > V$) which corresponds to a dispersion relation $k_0 = [\beta(\omega_0 - V)]^{1/2}$, where we have defined $\beta = (2m/\hbar)$ and $V = (V_0/\hbar)$. The Laplace transformed solution reads,

$$\bar{\psi}(x; p) = c_1 e^{ipx}, \quad x \geq 0, \quad (\text{A3})$$

where $p^2 = \beta(is - V)$. The corresponding Laplace transform of Eq. (1) yields

$$\bar{\psi}_0(0; s) = \frac{1}{s + i\omega_0}, \quad t > 0. \quad (\text{A4})$$

By combining Eqs. (A3) and (A4) evaluated at $x = 0$ we can determine the value of the constant c_1 , which yields the Laplace Transformed solution for $x \geq 0$,

$$\bar{\psi}(x; p) = \frac{e^{ipx}}{(p + k_0)(p - k_0)}, \quad x \geq 0. \quad (\text{A5})$$

The time dependent solution for $x > 0$ is readily obtained by performing the inverse Laplace transform of Eq. (A5), using the Bromwich integral formula,

$$\psi(x, t) = \frac{1}{2\pi i} \int_{\gamma' - i\infty}^{\gamma' + i\infty} \bar{\psi}(x; s) e^{st} ds, \quad (\text{A6})$$

where the integration path is taken along a straight line $s = \gamma'$ parallel to the imaginary axis in the complex s -plane. The real parameter γ' can be chosen arbitrarily as long as all singularities remain to the left-hand side of

$s = \gamma'$. After a simple partial fraction decomposition of in Eq. (A6) we obtain,

$$\psi(x, t) = \frac{1}{2\pi i} \left[\int_{\gamma' - i\infty}^{\gamma' + i\infty} \Phi_+(s) ds + \int_{\gamma' - i\infty}^{\gamma' + i\infty} \Phi_-(s) ds \right], \quad (\text{A7})$$

where the integrands $\Phi_{\pm}(s)$ are defined as,

$$\Phi_{\pm}(s) = \frac{i\beta}{2} \frac{e^{ipx} e^{st}}{p(p \pm k_0)}. \quad (\text{A8})$$

In order to evaluate the integral (A7) we perform the change of variable, $s' = s + iV$, which allows us to identify in Eq. (A7) the integral representation of the Moshinsky M -functions [8, 9]

$$M(x, \pm k_0, t) = \frac{1}{2\pi i} \int_{\gamma - i\infty}^{\gamma + i\infty} \frac{i\beta}{2} \frac{e^{i\sqrt{\beta}is'x} e^{s't}}{\sqrt{\beta}is'(\sqrt{\beta}is' \pm k_0)} ds', \quad (\text{A9})$$

and obtain the solution for the case of $\omega_0 > V$, given by Eq. (2). The solution for the case of $\omega_0 < V$, given by Eq. (3), is readily obtained along the same lines as Eq. (2).

1. Asymptotic behavior of the solutions

In this subsection we consider the long time behavior of the solutions given by Eqs. (2) and (3). This can be analyzed using the series expansion in powers of the argument y_q (Eq. (5)) of the M -functions (Eq. (4)) [9]. For large values of the argument y_q i.e. $|y_q| \gg 1$, the M -functions have the following series representation (see Ref. [9]):

$$M(y_q) \approx \frac{1}{2} e^{imx^2/2\hbar t} \left[\frac{1}{\pi^{1/2} y_q} - \frac{1}{\pi^{1/2} y_q^3} + \dots \right], \quad (\text{A10a})$$

provided that the phase, ϕ_q , of $y_q \equiv |y_q| \exp(\phi_q)$ lies in the interval $-\pi/2 < \phi_q < \pi/2$.

For the case $\pi/2 < \phi_q < 3\pi/2$, instead of Eq. (A10a) we have,

$$M(y_q) \approx \frac{1}{2} e^{imx^2/2\hbar t} \left[2e^{y_q^2} + \frac{1}{\pi^{1/2} y_q} - \frac{1}{\pi^{1/2} y_q^3} + \dots \right]. \quad (\text{A11a})$$

In general, the long time regime ($t \rightarrow \infty$) corresponds to large values of the argument y_q . For the particular values of $q = \pm iq_0$, we have that $y_q \rightarrow -e^{-i\pi/4}(t/\beta)^{1/2}q$. Note that this expression depends on the choice of q_0 , and by inspection, we can see that for the cases $q = iq_0$ and $q = -iq_0$ the arguments are $\phi_{iq_0} = -5\pi/4$ and $\phi_{-iq_0} = -\pi/4$, respectively. Therefore according to Eqs. (A10a) and (A11a), one obtains that in the limit $t \rightarrow \infty$,

$M(y_{-iq_0}) \rightarrow 0$ and $M(y_{iq_0}) \rightarrow e^{-q_0 x} e^{i(V-\omega_0)t}$. Substituting this values in Eq. (3) yields the asymptotic solution given by Eq. (6). By performing a similar analysis for

the case of wave evolution for $\omega_0 > V$ given by Eq. (2), one finds that the asymptotic behavior as $t \rightarrow \infty$ is given by Eq. (7).

- [1] K. W. H. Stevens, J. Phys. C: Solid State Phys. **16**, 3649 (1983).
- [2] P. Moretti, Physica Scripta **45**, 18 (1992).
- [3] N. Teranishi, A. M. Kriman and D. K. Ferry, Superlattices Microstruc. **3**, 509 (1987); A. P. Jauho and M. Jonson, *ibid.* **6**, 303 (1989); S. Brouard and J. G. Muga, Phys. Rev. A **54**, 3055 (1996).
- [4] M. Büttiker and H. Thomas, Superlattices Microstruc. **23**, 781 (1998); Ann. Phys. (Leipzig) **7**, (7) 602 (1998).
- [5] J. G. Muga and M. Büttiker, Phys. Rev. A **62**, 023808 (2000).
- [6] G. García Calderón, J. Villavicencio, F. Delgado, and J. G. Muga, Preprint arXiv: quant-ph 0206020 (2002).
- [7] A. D. Baute, I. L. Egusquiza and J. G. Muga, J. Phys. A: Math. Gen. **34**, 4289 (2001).
- [8] M. Moshinsky, Phys. Rev. **88**, 625 (1952); Am. J. Phys. **44**, (11) 1037 (1976).
- [9] G. García-Calderón and A. Rubio, Phys. Rev. A **55**, 3361 (1997).
- [10] *Handbook of Mathematical Functions*, edited by M. Abramowitz and I. A. Stegun (Dover, New York 1965), p. 297.
- [11] V. N. Faddeyeva and N. M. Terent'ev, *Tables of the Probability Integral for Complex Argument* (Pergamon Press, New York, 1961).
- [12] J. Villavicencio, J. Phys. A: Math. Gen. **33**, 6061 (2000).
- [13] G. García-Calderón and J. Villavicencio, Phys. Rev. A **64**, 012107 (2001).